Large-eddy simulation of pool fires with detailed chemistry using an unsteady flamelet model

By R. Rawat †, H. Pitsch and J. F. Ripoll

An unsteady flamelet approach is implemented as a subgrid combustion model for large-eddy simulation (LES) of buoyancy-dominated large-scale pool fires. In fires, soot plays a major role in the overall heat transfer, and therefore in the dynamics of fires. In simulations of soot formation in laminar flames, it has been shown that an accurate description is crucial to achieving reasonable predictions. Chemical reaction mechanisms accounting for the formation and oxidation of soot and of polycyclic aromatic hydrocarbons are typically described by hundreds of species and therefore are computationally expensive to incorporate if there is no simplification of the LES computation. Unsteady flamelet models permit consideration of detailed chemical kinetic mechanisms and a state-of-the-art description of soot formation and oxidation processes. The Lagrangian Flamelet model is incorporated in an existing LES fire code and compared with data from an experiment on a methane fire in a pool of one meter diameter. Results for soot predictions compare well with qualitative observations from the experiment. To discuss the influence of the description of radiative transport, a three-dimensional post-processing radiation simulation, using an averaged form of the M_1 radiation model with mean absorption coefficients, is also performed. For this latter simulation, distributions of temperature and of species volume fraction have been taken from the LES results.

1. Introduction

Accidental fires in the United States result in billions of dollars of property damage, and over 2000 deaths, per year. In the majority of accidental fires, the thermo-physical characteristics of the fuel are not sufficiently known to asses the fuel's fire safety properties, such as heat-release rate or effectiveness of fire-suppression agents. Also, experimental studies of large fires are hindered by monetary expense, sensitivity to environmental conditions, and harshness to diagnostic equipment. Numerical simulations provide a promising tool to complement experimental studies to further our understanding of fire safety and fire physics. The wide range of length and time scales present in large fires prohibits the use of three-dimensional direct numerical simulations. Also, accidental fires often involve the highly unsteady processes of fluid-structure interaction, flame spread across fuels, and wind effects. These processes will be better captured by large eddy simulations (LES) as opposed to Reynolds averaging approaches. Furthermore, in large pool fires, soot plays a major role in the overall heat transfer through radiation and therefore, in the dynamics of the fire. The solution of a full set of species transport equations, required by a detailed kinetic mechanism describing soot formation, is computationally unfeasible. An unsteady flamelet model is a viable approach to model chemistry/transport interactions allowing for the use of complex chemistry. This model has been developed by Pitsch *et al.* (1998) and has been applied to a series of momentum-driven reacting jets with good predictions of temperature and species mass fractions, including pollutants such as NO_x and

† University of Utah

soot. More recently, the model has been formulated for LES by Pitsch & Steiner (2000). In the present work, this model is incorporated into the LES fire code by Rawat *et al.* (2001). The model is applied in an LES of the experiment on a gaseous methane fire in a pool of one meter diameter by Tieszen *et al.* (2002), and compared with qualitative experimental observations and quantitative velocity data.

2. Numerical Formulation

The LES approach applied here in the numerical modeling of a pool fire is based on the set of spatially density-weighted filtered, time-dependent conservation equations for mass, momentum, mixture fraction, and enthalpy in a Cartesian coordinate system, given as (Moin *et al.* (1991))

$$\frac{\partial \bar{\rho}}{\partial t} + \nabla \cdot (\bar{\rho}\widetilde{\mathbf{u}}) = 0 \tag{2.1}$$

$$\frac{\partial \bar{\rho}\widetilde{\mathbf{u}}}{\partial t} + \nabla \cdot (\bar{\rho}\widetilde{\mathbf{u}}\widetilde{\mathbf{u}}) = -\nabla \bar{p} + \nabla \cdot \widetilde{\sigma} - \nabla \cdot (\bar{\rho}(\widetilde{\mathbf{u}\mathbf{u}} - \widetilde{\mathbf{u}}\widetilde{\mathbf{u}})) + (\rho - \rho_{\mathrm{ref}})\mathbf{g} \tag{2.2}$$

$$\frac{\partial \bar{\rho}\widetilde{Z}}{\partial t} + \nabla \cdot \left(\bar{\rho}\widetilde{\mathbf{u}}\widetilde{Z}\right) = \nabla \cdot (\bar{\rho}\widetilde{D_z}\nabla\widetilde{Z}) - \nabla \cdot \left(\bar{\rho}(\widetilde{\mathbf{u}Z} - \widetilde{\mathbf{u}}\widetilde{Z})\right) \tag{2.3}$$

$$\frac{\partial \bar{\rho}\widetilde{h}}{\partial t} + \nabla \cdot \left(\bar{\rho}\widetilde{\mathbf{u}}\widetilde{h}\right) = \nabla \cdot (\bar{\rho}\widetilde{\Gamma}\nabla\widetilde{h}) - \nabla \cdot \left(\bar{\rho}(\widetilde{\mathbf{u}h} - \widetilde{\mathbf{u}}\widetilde{h})\right) - \nabla \cdot \widetilde{\mathbf{q}}_{\mathrm{rad}} \tag{2.4}$$

Here, ρ is the density, t is the time, $\mathbf{u}$ is the velocity vector, p is the pressure, σ is the viscous stress tensor, Z is the mixture fraction, D_z is the molecular diffusion coefficient of the mixture fraction, h is the enthalpy, Γ is the thermal diffusion coefficient, and $\nabla \cdot \mathbf{q}_{\mathrm{rad}}$ is the net radiative heat flux. The hydrostatic pressure contribution from the pressure gradient is subtracted and combined with the buoyancy term to obtain $(\rho - \rho_{\mathrm{ref}})\mathbf{g}$. Pool fires can be described as low-speed flows where acoustic waves do not play a significant role in describing the dynamics. Therefore, the low-Mach-number variable-density formulation, as described by Najm *et al.* (1998), is used for the present calculations. These filtered equations are discretized on a 3-D, structured, Cartesian staggered grid using a second-order differencing scheme. An explicit, Runge-Kutta second-order time integration scheme is used for advancing the variables in time. The pressure equation for imposing mass conservation is obtained using the projection described by Najm *et al.* (1998). In their approach, the intermediate velocity is computed from the pressure-free momentum equation and then projected to satisfy the divergence-free constraint. The Poisson pressure equation obtained from this step is solved using Krylov methods. The intermediate velocity is then corrected by projecting it onto the calculated pressure field.

One of the important characteristics of the present fire scenario is that it occurs in an open domain. Pressure-based boundary conditions for fires, where crosswind is not important, are employed. At the inlet boundary, the boundary condition is a specified mass flux with a top hat velocity profile. At the lateral boundary, a traction-free boundary condition with a fixed specified pressure is used, allowing for air entrainment (Boersma *et al.* (1998)). At the outlet boundary a convective boundary condition as described by Akselvoll & Moin (1996) is specified.

The unresolved subgrid-scale Reynolds stress and the subgrid scalar fluxes are modeled using eddy-viscosity and eddy-diffusivity approaches. Thus the subgrid fluxes in the

momentum and mixture fraction transport equations are given by

$$\bar{\rho}(\widetilde{\mathbf{u}\mathbf{u}} - \widetilde{\mathbf{u}}\widetilde{\mathbf{u}}) = -2\bar{\rho}\nu_t\widetilde{\mathbf{S}} \tag{2.5}$$

and

$$\bar{\rho}(\widetilde{\mathbf{u}} - \widetilde{\mathbf{u}}\widetilde{Z}) = -\bar{\rho}D_t\widetilde{Z} \tag{2.6}$$

with

$$\widetilde{\mathbf{S}} = \frac{1}{2}((\nabla\widetilde{\mathbf{u}}) + (\nabla\widetilde{\mathbf{u}})^T)\,, \tag{2.7}$$

where ν_t is the subgrid kinematic eddy viscosity and D_t is the subgrid eddy diffusivity. The eddy viscosity ν_t is given by the Smagorinsky model as

$$\nu_t = C\Delta^2 \mid \widetilde{\mathbf{S}} \mid\,, \tag{2.8}$$

where C is the Smagorinsky coefficient and Δ is the filter width. The subgrid diffusivity D_t is determined from

$$D_t = \nu_t/\mathrm{Sc}_t\,, \tag{2.9}$$

where Sc_t is the turbulent Schmidt number, assumed to be a constant in the current calculation. Similarly, the turbulent diffusivity for the energy equation is computed assuming a constant turbulent Prandtl number. For the present calculations, the Smagorinsky coefficient is computed from the dynamic procedure and a value of 0.4 is used for both the turbulent Prandtl and Schmidt numbers as suggested by Pitsch & Steiner (2000). An assumed β-function PDF approach for the mixture fraction is used to compute the filtered density, temperature, and species mass fractions: this has been shown to be very accurate provided a good estimate of the subgrid mixture fraction variance (Cook & Riley (1994) and Wall *et al.* (2000)). The mixture fraction variance is modeled using the scale-similarity assumption.

3. Unsteady-flamelet model

An unsteady-flamelet approach is used to implement the complex chemistry mechanism described above. Formulation of the model follows the work of Pitsch & Steiner (2000) who applied this model in an LES of a momentum-dominated coflowing jet flame. This model has also been applied in RANS simulations of a sooting jet diffusion flame (Pitsch *et al.* (2000)). In these simulations it has been demonstrated that for predictions of NO_x and soot formation, the description of the slow underlying chemical and physical processes is important and therefore an unsteady flamelet model has to be used.

In the unsteady-flamelet approach, the state space variables are obtained by solving the one-dimensional unsteady laminar flamelet equations. As in steady-state flamelet equations parameters accounting for the influence of the turbulent flow field on the unsteady flame structure are required. In the current implementation, this coupling is based on the assumption that flamelets are introduced at the base of the pool fire inlet, and are convected downstream with the axial velocity at the stoichiometric mixture fraction. The flamelet time therefore corresponds to a Lagrangian-like lifetime of a portion of the flame within the flow field. While moving downstream, the flamelets experience different local scalar dissipation and radiative heat losses. Based on these assumptions, the flamelet time appearing in the unsteady term of the flamelet equations can be correlated to the distance from the nozzle. The scalar dissipation rate describing the effect of the turbulent flow field on the laminar flamelets is also required in the coupling of the flamelet

equations with the LES flow solver. All parameters are obtained by radially averaging the filtered quantities obtained from the flow solver, conditional on the mixture fraction.

The filtered scalar-dissipation rate is modeled using the assumption that on the subgrid scale, the scalar variance production and dissipation rates are in equilibrium, as proposed by Pierce & Moin (1998). The radiative heat loss is obtained by using the Rosseland model. Since this model becomes singular if the soot volume fraction tends to zero, an optically-thin gas model is used for $f_v < 5 \cdot 10^{-7}$. This assumption, however, is not expected to be very accurate for pool fires, where radiation is dominated by soot. The sensitivity of the results to this assumption will be discussed in the following section.

Current chemical-kinetic reaction mechanisms describing the formation and oxidation of polycyclic aromatic hydrocarbons (PAH) and soot are too large to be included directly in a fire simulation. Traditionally, soot chemistry has been incorporated into combustion simulations via an assumption of equilibrium gas-phase chemistry coupled with empirical correlations for soot volume fraction (Tien & Lee (1982)). In the past decade, researchers have devised various methods for including more detailed soot chemistry in combustion simulations. Fairweather *et al.* (1992) performed simulations of soot formation in turbulent jet flames by coupling flamelet libraries to a global reaction scheme for soot formation following the model of Leung *et al.* (1991) including soot nucleation, surface growth, particle coagulation, and oxidation steps. Belardini *et al.* (1996) modeled diesel engine combustion with a simplified six-step kinetic scheme which included both combustion and soot formation models. Brown & Fletcher (1996) described soot formation in 3-D coal combustion by solving gas phase transport equations for soot mass fraction and tar mass fraction. The rate of soot formation is based on the local tar mass fraction while soot and tar destruction are based on global one-step Arrhenius oxidation rates.

The chemistry model used in the present study to capture detailed soot kinetics is divided into three parts: a) The gas phase chemistry including 400 elementary reactions among 90 chemical species describing fuel oxidation, the formation of benzene, and the further growth to small PAHs consisting of up to four aromatic rings, b) a model for the growth of PAHs to possible infinite size, c) and a model describing the formation of particles from large PAHs, the further growth by heterogeneous surface reactions following an extended HACA mechanism, the oxidation of soot particles by O_2 and OH surface reactions, and particle-particle and particle-PAH coagulation processes. Flamelet equations are solved for the first two moments of the soot particle-size distribution, allowing for thermophoresis and differential diffusion effects. These models essentially follow the work of Frenklach & Harris (1987), Mauss et al. (1994) and Mauss (1998).

4. Radiation model

Because of the complexity of the simultaneous coupling of the turbulent combustion model, the soot model, and the radiation model, the large-eddy simulation results for the pool fire described in the next section have been obtained using a simplified radiation model. However, to assess the applicability of simplified models and to investigate radiative processes occurring in a turbulent fire, we have performed post-processing simulations using an instantaneous three-dimensional temperature distribution from the LES results, with a more sophisticated model for the radiative heat transfer, including emission and absorption by soot, gaseous water and carbon dioxide.

The macroscopic M_1 radiation model developed by Levermore (1984), Fort (1997), Dubroca & Feugeas (1999) and Brunner & Holloway (2001) is chosen here to describe

radiative heat transfer. The model is hyperbolic and the speed of propagation of disturbances is unlimited, which is different from the commonly-used diffusion models. The model also dissipates entropy locally. The M_1 model with mean absorption coefficients has been derived in Ripoll *et al.* (2001) to account for the frequency dependence of the opacity at a microscopic level. The mean absorption coefficients take the anisotropic form of the photon absorption into account, and lead to a better description of the photon flow away from radiative equilibrium. An averaged form of this model has been derived by Ripoll (2002) and Ripoll & Pitsch (2002). In this formulation, closure is achieved by assuming the anisotropy factor f and the radiative temperature T_R to be uncorrelated. Here, all radiative correlations, except for the contribution from soot emission, are neglected.

The M_1 radiation model describes the evolution of the radiative energy E_R and the radiative flux vector $\mathbf{F_R}$ of a non-scattering gray medium at temperature T.

$$\partial_t \overline{E}_R + \nabla \cdot \overline{\mathbf{F}}_\mathbf{R} = c\, C_s\, \overline{Y_s\, aT^5} - c\, C_s\, \overline{Y}_s\, \overline{G}_E\, \overline{T}_R\, \overline{E}_R + c\, \overline{C}_g^{\,e}\, a\, \overline{T}^4 - c\, \overline{C}_g^{\,a}\, \overline{E}_R, \tag{4.1}$$

$$\partial_t \overline{\mathbf{F}}_\mathbf{R} + c^2\, \nabla\, \left(\overline{\mathbf{D}}_\mathbf{R}\, \overline{E}_R\right) = -c\, C_s\, \overline{Y}_s\, \overline{G}_F\, \overline{T}_R\, \overline{\mathbf{F}}_\mathbf{R} - c\, \overline{C}_g^{\,a}\, \overline{\mathbf{F}}_\mathbf{R}, \tag{4.2}$$

The Eddington tensor $\overline{\mathbf{D}}_\mathbf{R}$ is defined by

$$\overline{\mathbf{D}}_\mathbf{R}(\mathbf{f}) = \mathbf{D}_\mathbf{R}(\overline{\mathbf{f}}) = \frac{1-\chi(\overline{\mathbf{f}})}{2}\, \mathbf{Id} + \frac{3\chi(\overline{\mathbf{f}})-1}{2}\, \frac{\overline{\mathbf{f}} \otimes \overline{\mathbf{f}}}{\|\,\overline{\mathbf{f}}\,\|}, \text{ with } \chi(\overline{\mathbf{f}}) = \frac{3+4\|\,\overline{\mathbf{f}}\,\|^2}{5+2\sqrt{4-3\|\,\overline{\mathbf{f}}\,\|^2}} \tag{4.3}$$

where $\mathbf{Id}$ is the identity matrix, $\overline{\mathbf{f}} = \overline{\mathbf{F}}_\mathbf{R}/(c\,\overline{E}_R)$ is the anisotropy factor, $\|\,.\,\|$ denotes an Euclidian norm, and χ is the Eddington factor. The radiative temperature, which represents an absorption temperature, is directly deduced from the radiative energy by $\overline{T}_R = \overline{E_R^{1/4}} = \overline{E}_R^{1/4}$.

The opacity, coming from the presence of the soot, is described through $C_s = 360 \frac{k\zeta_5}{\pi^4 h} C_1$ with $C_1 = 8.33 \times 10^{-9}$ (Lee & Tien (1981)). The opacity from gas radiation is given as $\overline{C}_g^{\,e} = C_g(\overline{T}, \overline{Y}_{\mathrm{H_2O}}, \overline{Y}_{\mathrm{CO_2}}) = C_{\mathrm{H_2O}}(\overline{T})\overline{Y}_{\mathrm{H_2O}} + C_{\mathrm{CO_2}}(\overline{T})\overline{Y}_{\mathrm{CO_2}}$ for emission and $\overline{C}_g^{\,a} = C_g(\overline{T}_R, \overline{Y}_{\mathrm{H_2O}}, \overline{Y}_{\mathrm{CO_2}})$ for absorption. The functions $C_{\mathrm{H_2O}}$ and $C_{\mathrm{H_2O}}$ are given elsewhere†. The anisotropy dependence of the mean absorption coefficients introduces the functions G_E and G_F in the absorption terms. These are given by

$$\overline{G}_E(\mathbf{f}) = G_E(\overline{\mathbf{f}}) = 1 + \frac{3}{4}\|\,\overline{\mathbf{f}}\,\|^2, \tag{4.4}$$

$$\overline{G}_F(\mathbf{f}) = G_F(\overline{\mathbf{f}}) = \frac{5}{4}(1 + \frac{1}{2}\|\,\overline{\mathbf{f}}\,\|^2). \tag{4.5}$$

The positive terms on the right-hand side of the M_1 model are the emission term while the negative terms represents those of absorption. The radiative net heat flux is given by the right hand side of 4.2. If full radiative heat transfer is considered, then this term also appears in the energy equation.

5. Results

Only pool fires around one meter in diameter and larger develop a fully turbulent flow, and only a few experiments have been done in this regime (Gritzo *et al.* (1998)). Tieszen

† www.ca.sandia.gov/tdf/Workshop/Submodels.html#Rad

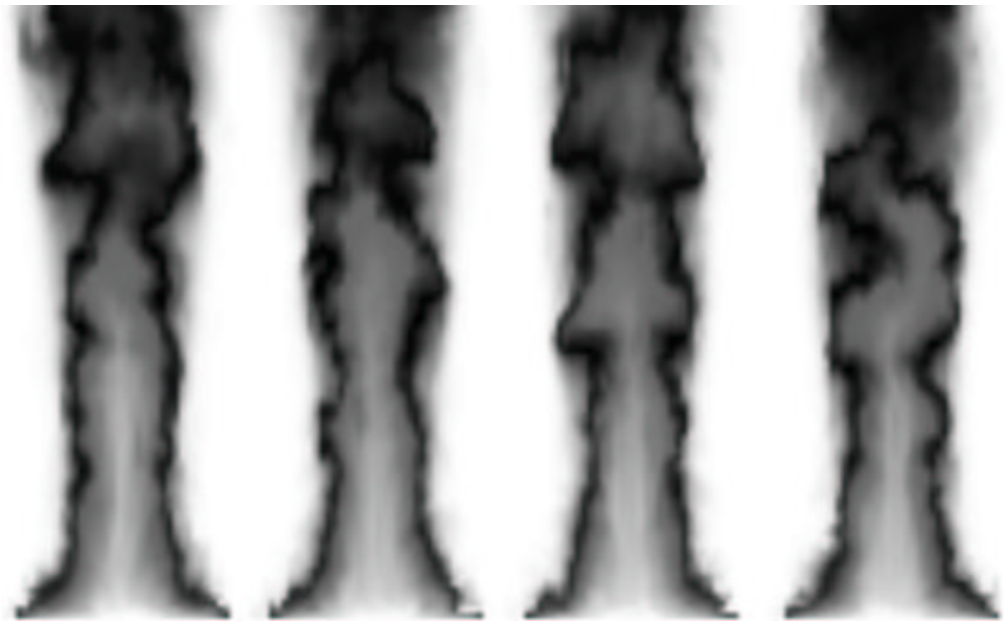

FIGURE 1. Instantaneous temperature contours of a one meter diameter methane fire at different times (increasing left to right), illustrating the puffing behavior of the pool fire.

et al. (2002) have studied a one-meter-diameter methane fire with boundary conditions and flow rate comparable to a large jet-fuel pool fire. The experimental data include averaged and instantaneous velocity fields close to the base of the fire. This experiment has been conducted to provide a database for validation of numerical simulations of pool fires. Soot volume fraction is validated qualitatively, based on general observations in this and other experiments.

The $3\,\mathrm{m}^3$ computational domain for the one-meter-diameter methane fire simulation was discretized into a uniform mesh of 100^3. The same computational mesh has been used for the radiation simulations. Figure 1 illustrates computed instantaneous temperature contours from longitudinal cross-sections at different times. The calculation demonstrates the capability of the fire simulation tool to capture the puffing nature of pool fires. The time sequence of one puff cycle illustrates the formation of a vortical structure at the toe of the fire that grows in size as it is convected downstream. These finger-like structures have been attributed to the baroclinic vorticity generation mechanism (Tieszen *et al.* (1996)). For buoyancy-dominated pool fires, this is the most important mechanism for the production of vortical structures. This time sequence also illustrates an initial vortex, formed at the toe, rolling up and breaking off from the main flame zone, which is consistent with the observation that an intermittent turbulent region follows a continuous flame region where most of the combustion takes place (Tieszen *et al.* (1996)). Figure 2 shows mean axial velocities at different axial locations compared with the experimental data. The simulation results capture the velocity trends well. However, the spreading rate is larger in the numerical simulation than was observed in the experiments. These differences might be attributed to several factors. First, mesh resolution is not fine enough to capture all the relevant large-scale, energy-containing eddies that control mixing, which leads to a wider spreading rate. Secondly, only a simple radiation model is used for the current calculations, which might not be accurate enough for pool fires As a result,

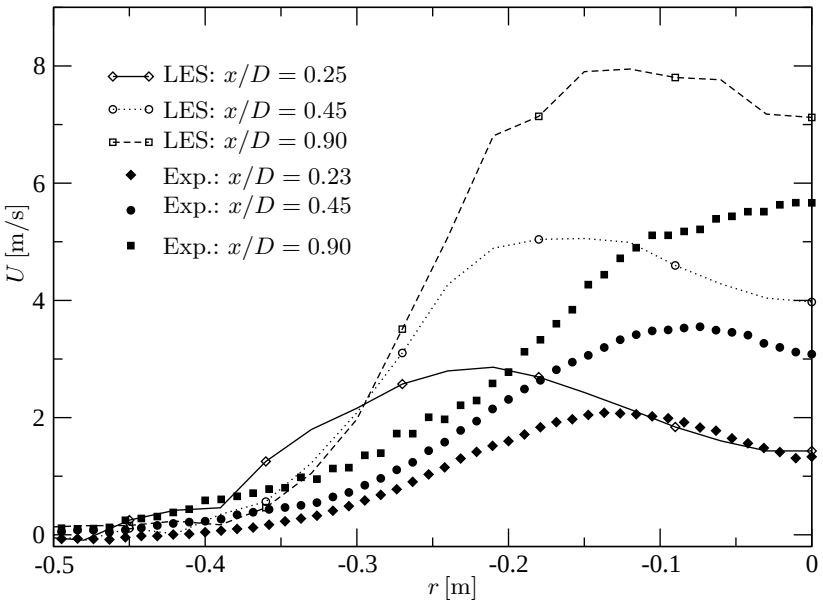

FIGURE 2. Comparison of radial time-averaged streamwise velocity profiles for a one-meter-diameter methane pool fire at different axial locations.

overall radiative emission from the simulated fire is lower than observed in real fires. Lower radiative emission produces higher fire temperatures, which leads to increased buoyancy and, consequently, higher velocities.

Figure 3 shows instantaneous soot volume fraction in a 2-D slice and a volume-rendered representation. The results indicate that soot is distributed throughout large regions of the flame, as is observed experimentally by Gritzo *et al.* (1998). The soot is completely oxidized before leaving the domain, which implies that there is no smoke formation in this fire. This is consistent with the experimental observation that smoke formation occurs only in pool fires larger than about 2 m in diameter. Radiative heat transfer for large-scale fires is dominated by emission and absorption, mainly from soot particles. To accurately predict radiative heat transfer from large scale fires, it is necessary to accurately predict local soot temperature and concentration. Time-averaged temperatures and soot volume fractions are shown in figure 4 at different axial locations. It is clearly seen that maximum soot concentration and maximum flame temperature do not occur at the same spatial location. Lower soot temperatures as seen in the figure have also been measured in experiments by Gritzo *et al.* (1998).

Figure 5 shows some results from a radiative calculation that has been done with a fixed instantaneous temperature field obtained from the LES. The radiative net heat flux shows that there is an absorption region in the center of the fire. A comparison with the soot volume-fraction distribution, shown in figure 3, indicates that because of the absence of soot in this region, the absorption here is caused by gaseous water and carbon dioxide. However, the regions of strong emission are governed mainly by

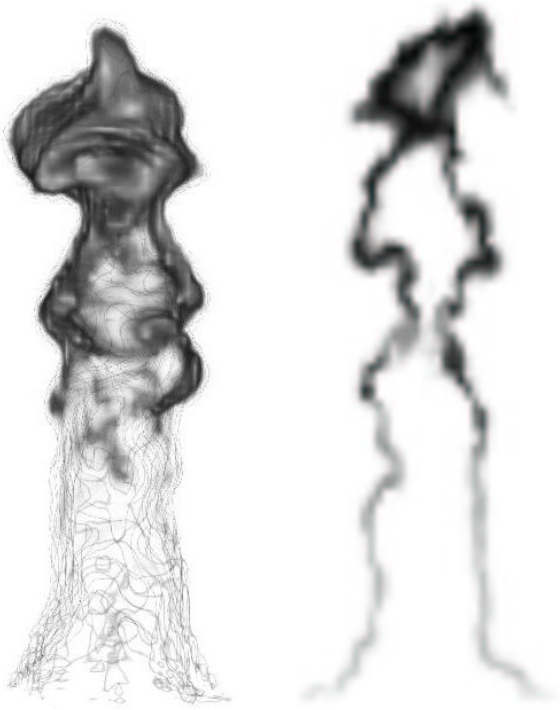

FIGURE 3. Instantaneous soot volume fraction at different times. The left figure shows a volume-rendered representation.

soot radiation. The M_1 model assures a transition of the anisotropy factor from $f = 0$, when radiation is isotropic, to its maximal value $f = 1$, when radiation is anisotropic. Isotropic regions are typically found in the central part of a fire, while the outside regions are usually anisotropic. This can also be observed in the present simulations, as shown in figure 5. Small values of the anisotropy factor usually indicate radiative equilibrium zones. Here, however, the small anisotropy in the center of the fire is due mainly to the symmetry about the centerline. Indeed, the radiative equilibrium, where emission balances absorption, $T \simeq T_R$, and hence $f = 0$, is almost never achieved for the present case. The thin radiative equilibrium zone can be identified T_R/T_m-field given in figure 5 as the region enclosed by the bold contour lines.

6. Conclusions

The Lagrangian Flamelet model has been successfully implemented for large-eddy simulation of buoyancy-dominated large-scale pool fires. The results from a one-meter-diameter methane pool fire simulation are compared with the experimental data for the time-averaged axial velocity field. The results capture the velocity trends well. The differences from the data have been attributed to the mesh resolution and the radiation model. Soot predictions from the simulations are in good agreement with the experimental observations for large-scale fires. Simulations also captured the negative spatial correlation between temperature and soot as seen in experiments. The importance of using a comprehensive three-dimensional radiative-transfer model for pool fires has been

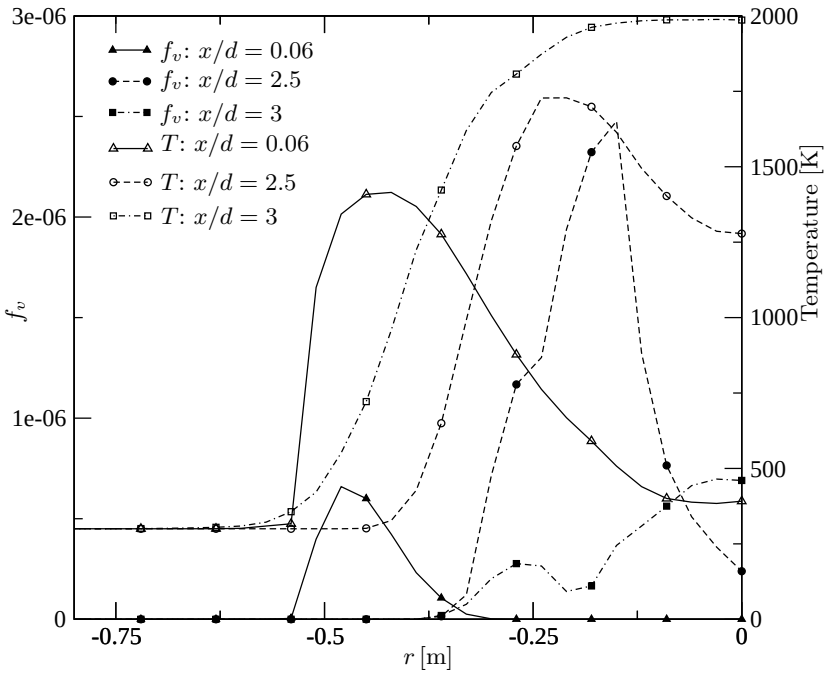

FIGURE 4. Radial time-averaged profiles of soot volume fraction and temperature for a one meter diameter methane pool fire at different axial locations

shown by comparing simulation results from the M_1 radiation model with the simplified radiation model.

REFERENCES

AKSELVOLL, K. & MOIN, P. 1996 Large-eddy simulation of turbulent confined annular jets. *J. Fluid Mech.* **315**, 387–411.

BILGER, R. 1980 Turbulent flows with nonpremixed reactants. *Topics in Applied Physics: Turbulent Reacting Flows* (P. A. Libby and F. A. Williams, eds.), Springer, Berlin, 65–113.

BOERSMA, B. J., BRETHOUWER, G. & NIEUWSTADT, F. T. M. 1998 A numerical investigation on the effect of the inflow conditions on the self-similar region of a round jet. *Phys. Fluids* **10**, 899–909.

BELARDINI, P., BERTOLI, C., BEATRICE, C., D'ANNA, A. & DEL GIACOMO, N. 1996 Application of a reduced kinetic model for soot formation and burnout in three-dimensional diesel combustion computations. *Proc. Combust. Inst.* **26**, 2517–2524.

BROWN, A. L. & FLETCHER, T. H. 1996 Modeling soot in coal combustion flames. *Western States Section of the Combust. Inst.*

BRUNNER, T. A. & HOLLOWAY, J. P. 2001 One-dimensional Riemann solvers and the maximum entropy closure. *J. Quant. Spectrosc. Radiat. Transfer* **69**, 543–566.

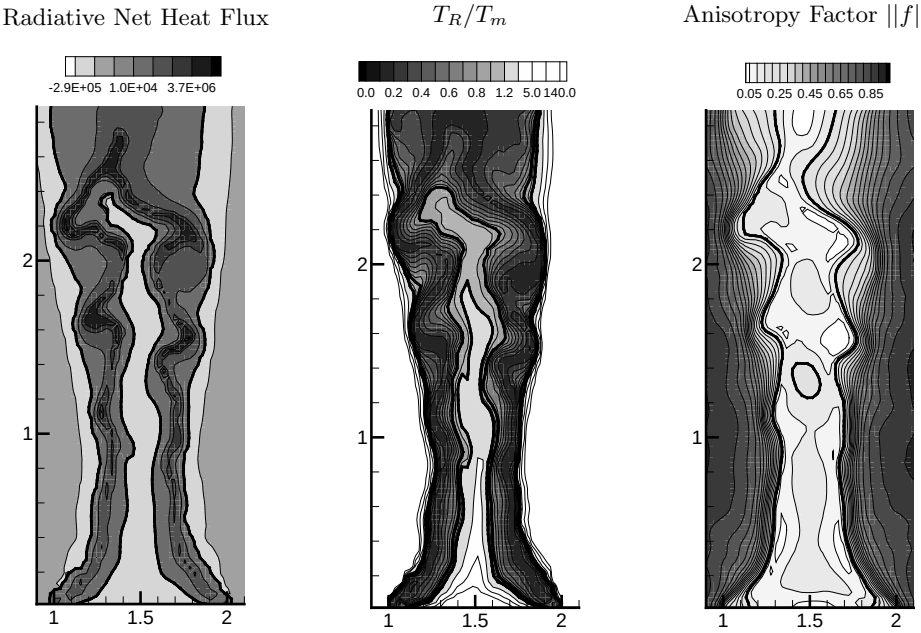

FIGURE 5. Net radiative heat flux, ratio of radiative to matter temperature T_R/T_m, and norm of the anisotropy factor $||f||$. Bold lines indicate zero net radiative heat flux in the left, $T_R/T_m = 0.8$ and $T_R/T_m = 1.2$ in the middle, and $||f|| = 0.2$ in the right figures.

COOK, A. W. & RILEY, J. J. 1994 A subgrid model for equilibrium chemistry in turbulent flows. *Phys. Fluids* **6**, 2868–2870.

DUBROCA, B. & FEUGEAS, J.-L. 1999 Etude théorique et numérique d'une hiérarchie de modèles aux moments pour le transfert radiatif. *C. R. Acad. Sci. Paris* **329**, 915–920.

FAIRWEATHER, M., JONES, W. P., LEDIN, H. S. & LINDSTEDT, R. P. 1992 Predictions of soot formation in turbulent, non-premixed propane flames. *Proc. Combust. Inst.* **24**, 1067–1074.

FORT, J. 1997 Information-theoretical approach to radiative transfer. *Phys. A.* **243**, 275–303.

FRENKLACH, M. & HARRIS, S. J. 1987 Aerosol dynamics modeling using the method of moments. *J. Coll. Interf. Sci.* **118**, 252–261.

GRITZO, L. A., SIVATHANU, Y. R. & GILL, W. 1998 Transient measurements of radiative properties, soot volume fraction and soot temperature in a large pool fire. *Combust. Sci. and Tech.* **139**, 113–136.

LEE, S. C. & TIEN, C. L. 1981 Optical constants of soot in hydrocarbon flames. *Proc. 18th International Symposium on Combustion.* The Combustion Institute, 1159–1166.

LEUNG, K. M., LINDSTEDT, R. P. & JONES, W. P. 1991 *Combust. Flame* **87**, 289–305.

LEVERMORE, D. 1984 Relating Eddington factors to flux limiters. *J. Quant. Spectrosc. Radiat. Transfer*, **31**, 149–160.

MAUSS, F., TRILKEN, B., BREITBACH, H. & PETERS, N. 1994 Soot formation in par-

tially premixed diffusion flames at atmospheric pressure. *Soot Formation in Combustion*, (H. Bockhorn, ed.), Springer, Berlin, 325–349.

Mauss, F. 1998 Development of a kinetic soot model for soot formation with fast polymerization. *Ph.D Thesis*, RWTH Aachen.

Najm, H. N., Wyckoff, P. S. & Knio, O. M. 1998 A semi-implicit numerical scheme for reaction flow: 1. Stiff chemistry. *J. Comput. Phys.* **143**, 389-406.

Moin, P., Squires, K., Cabot, W. & Lee, S. 1991 A dynamic subgrid-scale model for compressible turbulence and scalar transport. *Phys. Fluids* **3**, 2746–2757.

Pierce, C. D. & Moin, P. 1998 A dynamic model for subgrid-scale variance and dissipation rate of a conserved scalar. *Phys. Fluids* **10**, 3041–3044.

Pitsch, H., Chen, M. & Peters, N. 1998 Unsteady flamelet modeling of turbulent hydrogen/air diffusion flames. *Proc. Comb. Inst.* **27**, 1057–1064.

Pitsch, H. & Steiner, H. 2000 Large-eddy simulation of a turbulent piloted methane/air diffusion flame (Sandia flame D). *Phys. Fluids* **12**, 2541–2554.

Pitsch, H., Riesmeier, E. & Peters, N. 2000 Unsteady flamelet modeling of soot formation in turbulent diffusion flames. *Combust. Sci. and Tech.,* **158**, 389–406.

Rawat, R., Parker, S. G., Smith, P. J. & Johnson, C. R. 2001 Parallelization and integration of fire simulations in the Uintah PSE. *Proc. 10th SIAM Conference on Parallel Processing for Scientific Computing, Portsmouth, VA.*

Ripoll, J.-F., Dubroca, B. & Duffa, G. 2001 Modelling radiative mean absorption coefficients. *Comb. Theory and Mod.* **5**, 261–275.

Ripoll, J.-F., Dubroca, B. & Audit, E. 2002 A factored operator method for solving coupled radiation-hydrodynamics models. Preprint, to appear in Trans. Theor. and Stat. Phys.

Ripoll, J.-F. 2002 An averaged formulation of the M_1 radiation model with presumed probability density functions for turbulent flows. Preprint, submitted for publication.

Ripoll, J.-F. & Pitsch, H. 2002 Modelling turbulence-radiation interactions for large sooting turbulent flames. Preprint.

Tien, C. L. & Lee, S. C. 1982 Flame radiation. *Prog. Energy Combust. Sci.* **8**, 41–59.

Tieszen, S. R., Nicolette, V. F., Gritzo, L. A., Holen, J. K., Murray, D., & Moya, J. L. 1996 Vortical structures in pool fires: observation, speculation, and simulation. *Sandia National Lab. Report No.* SAND96–2607.

Tieszen, S. R., O'Hern, T. J., Schefer, R. W., Weckman, E. J. & Blanchat, T. K. 2002 Experimental study of the flow field in and around a one meter diameter methane fire. *Combust. and Flame,* **129**, 378–391.

Wall, C., Boersma, B. J. & Moin, P. 2000 An evaluation of the assumed beta PDF subgrid-scale model for LES of non-premixed, turbulent combustion with heat release.*Phys. Fluids* **12**, 2522–2529.